Extracting Curve Skeletons from Gray Value Images for Virtual Endoscopy.

Conference Paper · January 2008

Source: DBLP

2 authors, including:

Horst Bischof
Graz University of Technology
731 PUBLICATIONS **14,438** CITATIONS

SEE PROFILE

Extracting Curve Skeletons from Gray Value Images for Virtual Endoscopy*

Christian Bauer and Horst Bischof

Institute for Computer Graphics and Vision, Graz University of Technology, Austria
{cbauer, bischof}@icg.tu-graz.ac.at

Abstract. The extraction of curve skeletons from tubular networks is a necessary prerequisite for virtual endoscopy applications. We present an approach for curve skeleton extraction directly from gray value images that supersedes the need to deal with segmentations and skeletonizations. The approach uses properties of the Gradient Vector Flow to derive a tube-likeliness measure and a medialness measure. Their combination allows the detection of tubular structures and an extraction of their medial curves that stays centered also in cases where the structures are not tubular such as junctions or severe stenoses. We present results on clinical datasets and compare them to curve skeletons derived with different skeletonization approaches from high quality segmentations. Our approach achieves a high centerline accuracy and is computationally efficient by making use of a GPU based implementation of the Gradient Vector Flow.

1 Introduction

Modern volumetric imaging techniques provide detailed information about tubular structures such as colon, blood vessels, or the bronchial tree. To make use of this information virtual endoscopy (VE) systems can be used. These systems have become powerful tools for aiding procedures such as diagnosis, preoperative planning, or intraoperative support. To achieve this, VE combines methods of medical image understanding with virtual reality methods and typically involves three tasks: 1) Identification/segmentation of the interesting structures in the volumetric dataset. 2) Extraction of the associated curve skeleton (CS) representing the flight paths through the tubular networks. 3) Visualization of the interesting structures from points on the given flight paths using isosurface or other volume rendering techniques.

The first two tasks are usually treated separately - segmentation with a consecutive skeletonization. There are robust general purpose methods for extraction of CSs from discrete objects that can be used application independent [1,2,3,4]; however, the segmentation methods are typically application dependent, require manual initialization, or adaption of parameters. Methods that extract centerlines directly from gray value images on the other hand are rare and either

* This work was supported by the Austrian Science Fund (FWF) under the doctoral program Confluence of Vision and Graphics W1209.

T. Dohi, I. Sakuma, and H. Liao (Eds.): MIAR 2008, LNCS 5128, pp. 393–402, 2008.

require specification of start- and endpoints of the flight path [5,6] - for highly branched tubular structures such as the bronchial tree this is difficult - or they are based on tube detection approaches [7,8,9]. These methods have problems to extract valid centerlinepaths in proximity of junctions or diseases like stenosis and require additional postprocessing steps that do not guarantee centered paths [10,8,11].

In a previous work we used the Gradient Vector Flow (GVF) [13] for identification of tubular objects as a replacement for the multi-scale gradient vector computation used by most tube detection filters [12]. In combination with Frangi's vesselness measure [9] the overall approach allows detection of tubular objects (more precisely their centerlines) independent of the tubes size and contrast and the method shows a high robustness against image noise and disturbances outside the tubular objects. But similar to other tube detection filters the method does not produce valid centerline paths in the proximity of junctions or diseases like stenosis where the objects are not tubular. However, the GVF shows another property that can be used to solve this problem and that has been used for extraction of CSs from binary segmentations by the skeletonization approach of Hassouna and Farag [2]. In contrast to skeletonization approaches that are based on the distance transformation the magnitude of the GVF is always guaranteed to vanish at the medial curves independent of the object's shape. This enables the extraction of the centerlines also in case of junctions or plate like structures.

In this work, we present a system for extraction of complete CSs from tubular networks directly from gray value images. This supersedes the need to deal with two problems - segmentation and skeletonization. We propose to use the GVF's properties in two ways: first, for detection of tubular objects and thus selection of the interesting structures. Second, for extraction of the complete medial curves that stay centered also in case of junctions or diseases. This approach combines the advantages of tube detection filters - their robustness against leakage and their ability to detect small low contrast structures - with the advantage of Hassouna and Farag's skeletonization approach - its ability to extract centered lines also in areas where the objects are not tubular. The proposed approach may be used in several application areas and not just VE applications, but, as it extracts centered paths, it is especially suited for VE applications. It is further computationally efficient - as it uses the GVF as a core component similar to Hassouna and Farag's skeletonization approach - and may perform fully automatic for some application domains since it performs a bottom up detection of tubular objects for identification of the interesting structures.

2 Methodology

The basic idea of our approach is outlined in Fig. 1 for some simple 3D tubular objects. The approach consists of three processing steps: 1) Performing the GVF on the gray value image. 2) Identification of tubular objects. 3) Extraction of the medial curves that are associated with tubular objects (thus not only the

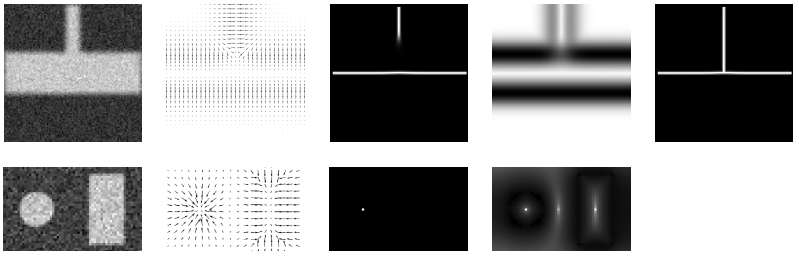

Fig. 1. Illustration of the basic idea on 2D cross section profiles of some 3D structures. Top row: cross section T-junction of a tubular object; bottom row: tube and plate like structures. From left to right: original dataset, GVF, derived tube-likeliness, derived medialness (after appropriate weighting for visualization purposes), extracted CS.

tubular part is extracted, but also areas of stenoses/aneurisms or junctions are handled).

Gradient Vector Flow: The first step of the processing pipeline is performing the GVF on the gray value image. This allows an edge-preserving diffusion of gradient information from the boundaries towards the centers of the interesting structures.

Depending on the application domain the initial gradient information is obtained differently: $F = \nabla(G_\sigma \star I)$ for structures surrounded by darker tissue (e.g. angiography images), $F = -\nabla(G_\sigma \star I)$ for structures surrounded by brighter tissue (e.g. airways), $F = -\nabla|\nabla(G_\sigma \star I)|$ for structures surrounded by arbitrary step edges (e.g. blood vessels containing calcifications), whereby I is the original image and G_σ is a Gaussian filter kernel with a given variance (we used a variance of one voxel in all presented experiments). In contrast to other tube detection filters the gradient information is obtained only on a small scale that only accounts for image noise. We do not require multiple scales which may result in an undesired diffusion of nearby structures into one another on larger scales. This would influence the detection of tubular objects and the accuracy of the associated centerlines [12].

The given initial gradient information is normalized to account for varying contrast situations, $F^n(\mathbf{x}) = F(\mathbf{x})/|F(\mathbf{x})| * (min(|F(\mathbf{x})|, F_{max})/F_{max})$ where $\mathbf{x} = (x, y, z)$, and used to initialize the GVF. The GVF as proposed by Xu and Prince [13] is defined as the vector field $V(\mathbf{x})$ that minimizes:

$$E(V) = \iiint_\Omega \mu|\nabla V(\mathbf{x})|^2 + |F^n(\mathbf{x})|^2|V(\mathbf{x}) - F^n(\mathbf{x})|^2 d\mathbf{x}, \tag{1}$$

where μ is a regularization parameter that usually has to be adapted according to the amount of noise. We use the normalized gradient vector information F^n to account for varying noise levels (σ) and contrast levels (F_{max}) as these parameters are more intuitive to set than the GVF's regularization parameter.

Thus, we used a fixed value of $\mu = 0.5$ in all presented examples. The variational formulation of the GVF makes the result smooth where the initial vector magnitudes are small, while keeping vectors with high magnitude nearly equal. This allows an edge-preserving diffusion of gradient information from boundaries towards the centers of the structures of interest (see Fig. 1).

Identification of tubular objects: At the centers of tubular objects the vector field derived from the GVF shows the same characteristic properties that are used by other tube detection filters for identification of tubular objects (see Fig. 1): All vectors point directly towards the centerline of the tubular object; they show a large variance in two dimensions and a low variance in the third dimension. Therefore, the GVF can be used a replacement for the multi-scale gradient vector computation performed by other tube detection filters [12].

To derive a tube-likeliness from these vectors $V^n(\mathbf{x}) = V(\mathbf{x})/|V(\mathbf{x})|$ the Hessian matrix $H(\mathbf{x}) = \nabla V^n(\mathbf{x})$ with its eigenvalues $|\lambda_1| \leq |\lambda_2| \leq |\lambda_3|$ can be used. Currently we are using Frangi's vesselness measure [9] to derive the final tube-likeliness from these eigenvalues since it is simple and well known:

$$T(\mathbf{x}) = \begin{cases} 0 & \text{if } \lambda_2 > 0 \text{ or } \lambda_3 > 0 \\ \big(1 - exp\big(-\frac{R_A^2}{2\alpha^2}\big)\big) exp\big(-\frac{R_B^2}{2\beta^2}\big) \big(1 - exp\big(-\frac{S^2}{2c^2}\big)\big) & otherwise \end{cases} \tag{2}$$

with $R_A = |\lambda_1|/\sqrt{|\lambda_2||\lambda_3|}$ indicating blob-like structures, $R_B = |\lambda_2|/|\lambda_3|$ to distinguish between plate-like and line-like structures, and $S = \sqrt{\lambda_1^2 + \lambda_2^2 + \lambda_3^2}$ for suppression of random noise effects. The parameters α, β, and c allow to control the sensitivity of the filter to the measures R_A, R_B, and S, respectively. In combination with our approach the third term of Frangi's vesselness measure that controls the noise-sensitivity becomes obsolete since noise is already suppressed. Also for the other parameters Frangi's suggested default values are used: $\alpha = 0.5$, $\beta = 0.5$, and $c = 100$.

The overall combination of the GVF with Frangi's vesselness measure allows detection of tubular objects (more precisely their centerlines), whereby the response is independent of the tubes size and contrast (see Fig. 1). But similar to other tube detection filters it does not produce valid centerlines where the objects are not tubular such as in areas of junctions or diseases like stenoses where the cross section profile is more plate-like.

Medial curve extraction: As outlined in the introduction, the magnitude of the GVF vanishes at medial curves also for non-tubular objects and this property can be used to extract the complete medial curves of identified tubular objects also in areas where the tubes do not show a circular cross-section.

The magnitude of the GVF vanishes towards the centers of the objects but it not necessarily becomes zero. As a measure of medialness we use $M(\mathbf{x}) = 1 - |V(\mathbf{x})|$. Fig. 1 shows the derived medialness after an appropriate weigthing (this weighting is only used for visualization but not for computation). In the so derived medialness map medial curves form height-ridges that can be extracted. We use a height ridge traversal procedure for this purpose for two main reasons:

first, it is computationally highly efficient (see Sec. 3). Second, it allows immediate extraction of a higher-level representation that describes the complete CS including the centerlines, junction points, and connectivity information between the single tubular objects.

Given the medialness map M and a starting point $\mathbf{x}_0$ on a height-ridge the complete associated medial curve can be extracted using a procedure similar to the method suggested by Aylward and Bullit [7]. This procedure needs an estimate of the ridge orientation $\mathbf{t}(\mathbf{x})$; we obtain this information from the Hessian matrix as the eigenvector associated with its smallest eigenvalue. Thus, given a starting point $\mathbf{x}_0$ the heigh-ridge is traversed into both directions $\mathbf{t}(\mathbf{x}_0)$ and $-\mathbf{t}(\mathbf{x}_0)$. For a current point on the height ridge $\mathbf{x}_i$ all local neighbors $\mathbf{x}_i^n$ with $\overrightarrow{\mathbf{x}_i\mathbf{x}_i^n} \cdot \mathbf{t}_i > 0$ are considered and the neighbor with the highest medialness is chosen as the next point $\mathbf{x}_{i+1}$ on the medial curve. The tangent direction $\mathbf{t}(\mathbf{x}_{i+1})$ is set to $\mathbf{t}(\mathbf{x}_{i+1}) = \text{sign}(\overrightarrow{\mathbf{x}_i\mathbf{x}_{i+1}} \cdot \mathbf{t}(\mathbf{x}_{i+1}))\mathbf{t}(\mathbf{x}_{i+1})$ to maintain the correct direction during traversal and the procedure is repeated until a stopping criterion is met. The procedure it stopped when the medialness falls below a given threshold m_{min} (an endpoint of the medial curve is found; we used $m_{min} = 0.1$ in all presented experiments) or an already traversed point is found (a junction of two medial curves is found). This way the complete medial curves are extracted.

Combination: The final step is to combine the results of the last two steps: we use the tube-likeliness for identification of the interesting structures and the medial curve extraction to obtain the complete centerlines associated with the tubular structures.

This requires specification of starting points for the height-ridge traversal procedure. As we know that the tube-likeliness increases for tubular structures and that the response falls off in proximity of junctions, we can conclude that every tubular object contains at least one local maximum in the tube-likeliness map. Thus all local maxima in the tube-likeliness map with a value $T(\mathbf{x}) > T_{min} = 0.5 * \max_{y \in \Omega} T(\mathbf{y})$ are considered as starting points for the height-ridge traversal (for robustness reasons these starting points are processed in descending order of their associated tube-likeliness). However, as the tube detection filter may produce some short spurious responses due to noise one further condition is necessary; the direct neighbors of the candidate starting points along the height-ridge also have to be tubular ($T(\mathbf{x}) > T_{min}$). This strategy discards short spurious responses and is comparable with pruning strategies used with other skeletonization approaches [1,4] or tube extraction methods [10].

Applying this procedure allows a bottom up detection of the complete medial curves associated with tubular objects that is robust to local variations along the tube such as junctions, stenoses, or aneurisms. As the height-ridge traversal also provides connectivity information between the single medial curves, the complete CSs of the tubular networks are also known immediately and in some application domains the structure of interest can be identified as the largest connected component (concerning its centerline length).

3 Evaluation

In this section we present results achieved on clinical datasets and compare them quantitatively and qualitatively to other methods with similar objectives. We will show two things: first, our approach is able to extract medial curves that stay centered also in complicated cases where pure tube detection filters have problems; we do this by comparing our approach to results achieved with another approach that extracts medial curves directly from the gray value images [8,10]. Second, the accuracy of the extracted centerlines is comparable to those achieved with pure skeletonization approaches from accurate segmentations; we do this by comparing the results of our approach to the skeletons extracted with three different skeletonization approaches [2,4,1] from known gold standards (available segmentations of the interesting structures).

Datasets and methods: The three clinical datasets we used for evaluation show a bronchial tree (see Fig. 2), a contrast CT of an aorta containing a severe stenosis due to calcification (see Fig. 3), and a CT angiography image of the brain (see Fig. 4). High quality segmentations of the bronchial tree and the aorta were available; the segmentation of the aorta follows the interior of the aorta excluding the calcifications. For the CTA of the brain only a low quality segmentation based on thresholding was available.

The approaches we used for comparison are three sophisticated skeletonization approaches (using binary segmentations) that were presented for VE applications and one method that derives the medial curves directly from the gray

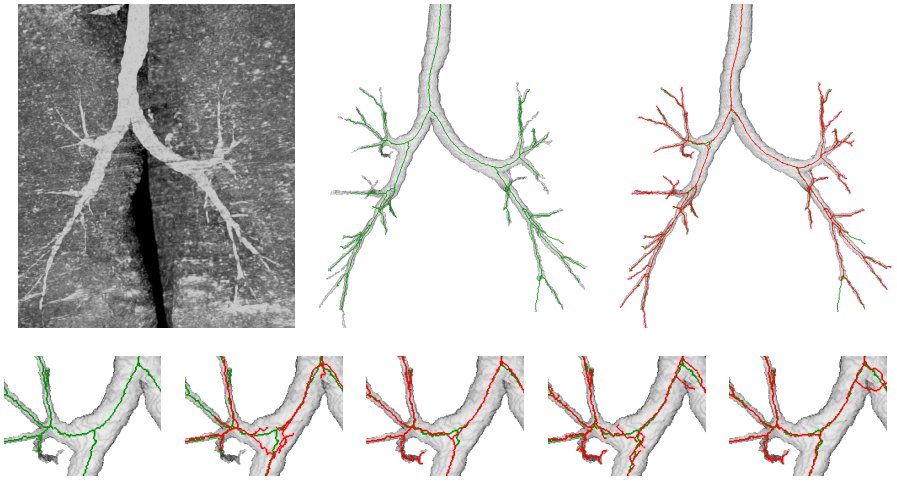

Fig. 2. Airway tree and resulting CSs. Top row (overview): volume rendering of the original dataset, CS of the proposed approach and Hassouna's approach. Bottom row (subregion around a junction): CS of the proposed approach, Krissian's approach, Hassouna's approach, Bouix's approach, and Palagyi's approach (green: proposed approach; red: other approaches).

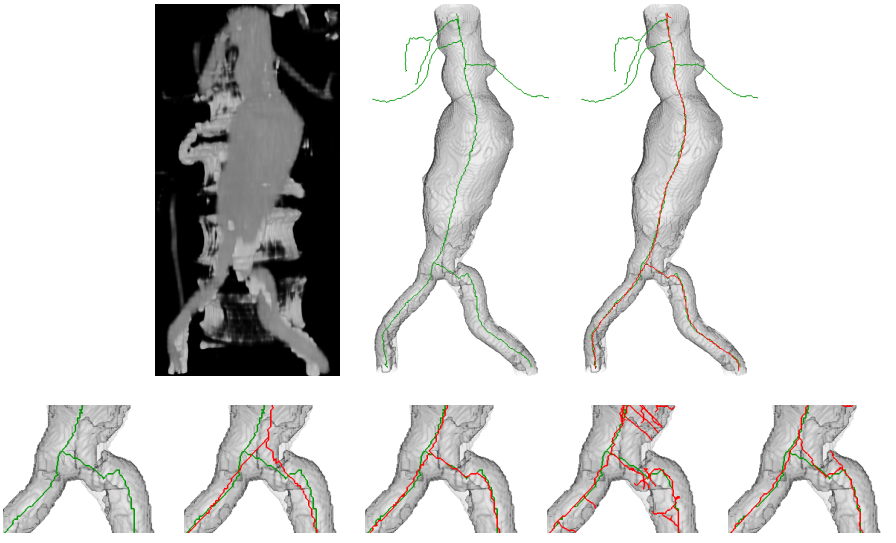

Fig. 3. Contrast CT dataset of the aorta containing a severe stenosis due to calcification. Top row (overview): volume rendering of the original dataset, CS of the proposed approach and Hassouna's approach. Bottom row (subregion around the stenosis): CS of the the proposed approach, Krissian's approach, Hassouna's approach, Bouix's approach, and Palagyi's approach (green: proposed approach; red: other approaches).

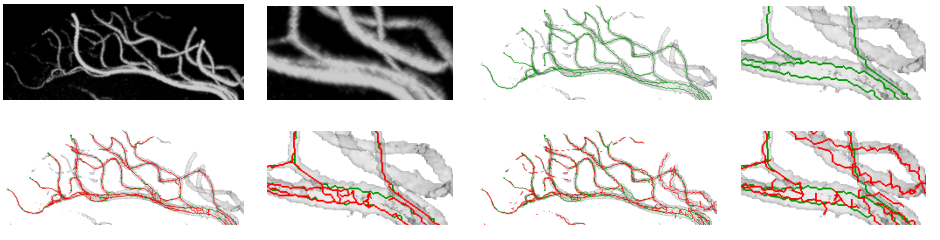

Fig. 4. CT angiography dataset of the brain and resulting CSs. Shown are a subbranch of the dataset and a subregion with some closely adjacent vessels. From left to right, from top to bottom: MIP of the original dataset, CS of the proposed approach, Krissian's approach, and Hassouna's approach (green: proposed approach; red: other approaches).

value image. The skeletonization approaches are that of Hassouna et al. [2,3], Bouix et al. [4], and Palagyi et al. [1]. Hassouna's approach also uses the GVF similarly to our approach; the other two methods were specifically developed for tubular objects. As a representative example of a method that tries to extract centerlines directly from gray value images we decided to use a combination of the methods of Krissian et al. [8] (for a bottom up detection of tubular structures) and Bullitt et al. [10] (for grouping the single tubular objects into tree structures and an extraction of the complete CS). For all approaches the

authors default parameters were used. For our approach the initialization of the GVF had to be set appropriately depending on the application domain (tubes surrounded by brighter/darker tissue and the expected contrast level F_{max}; see Sec. 2); the CSs were extracted fully automatic without any user interaction by identifying the largest connected component as described in Sec. 2.

Qualitative Results: In Figs. 2, 3, and 4, the results achieved with our approach and the other methods on the three clinical datasets are shown.

The airway dataset (see Fig. 2) demonstrates that the results of the different methods for the standard case - one tubular object - of all methods are almost identical. But at one of the junctions that shows a larger variation from the typical shape (it becomes more plate like) some approaches had problems to produce valid centerlines. In particular, the combined approach of Krissian and Bullit had problems since this combination does not guarantee centered paths in junction areas. The completeness of the resulting CS achieved with our approach is also comparable to that of the gold standard.

On the aorta dataset (see Fig. 3) the different methods show the major differences at the junction with the stenotic area. Krissian's multi-scale tube detection filter was influenced by the calcification and thus the resulting centerline moved far away from the desired position. Our approach was able to extract a medial curve that stayed centered in proximity of the stenosis with a quality comparable to that of the skeletonization approaches. The approaches of Bouix and Palagyi showed some sensitivity to surface noise and produced additional centerlines; the authors themselves mention this behaviour and these spurious branches can be removed by appropriate pruning strategies.

On the CTA of the brain (see Fig. 4) closely tangenting vessels with diffuse boundaries and thin low contrast vessels are typically the difficult situations for segmentation methods/tube detection filters. Krissian's approach had problems to extract valid centerlines for the closely tangenting vessels. Contrary, our approach successfully separated them and extracted valid centerlines for these structures. Further, our approach was also able to extract most of the thin low contrast vessels similarly to Krissian's tube detetion filter. As only a low quality segmentation was available none of the skeletonization approaches was able to extract valid centerlines for the tangenting vessels; therefore we show only the result of one of the skeletonization methods.

Quantitative Results: The quantitative comparison of the centerline accuracy is based on the average centerline distances between the different methods. To make the CSs comparable, the skeletons obtained with the methods of Bouix and Palagyi were pruned and only branches detected by all methods (the segmenation methods and the tube detection filter methods) were considered. Table 1 summarizes the average centerline distances between the different methods for the two datasets with the high-quality segmentations. All the methods are quite comparable (except the results achieved with the combined approach of Krissian and Bullitt). Most notably is the small difference between our proposed method and Hassouna's approach on the airway tree, but this may be explained since both methods are based on the GVF. As these results show, the achieved

Table 1. Average centerline distances (in voxels) between the CSs extracted with different approaches from the bronchial tree and the aorta dataset

	Bronchial Tree					**Aorta**				
	M1	M2	M3	M4	M5	M1	M2	M3	M4	M5
proposed (M1)	–	0.24	0.41	0.40	0.58	–	0.66	0.62	0.79	1.49
Hassouna (M2)	0.22	–	0.37	0.34	0.72	0.63	–	0.60	0.72	1.14
Bouix (M3)	0.47	0.36	–	0.45	0.67	0.59	0.63	–	0.78	1.58
Palagyi (M4)	0.44	0.33	0.44	–	0.70	0.78	0.75	0.80	–	1.53
Krissian (M5)	0.59	0.53	0.57	0.66	–	1.61	1.17	1.70	1.60	–

centerline accuracy of our proposed method is comparable to the variation found between different skeletonization approaches; and this although all the skeletonization approaches use the same binary segmentations while our method does not know this gold standard. This proofs that our approach is able to extract CSs of comparable quality directly from the gray value images.

Implementational and computational effort: Our current implementation is based mainly on standard ITK-Filters[1] and a GPU based implementation of the GVF using the CUDA Framwork[2] as the main computational effort is due to the GVF. This allows an efficient computation of the GVF (500 iterations): $150 \times 110 \times 60$ voxels in ~ 3 seconds; $256 \times 256 \times 256$ voxels in ~ 15 seconds; $380 \times 210 \times 425$ voxels in ~ 30 seconds on an NVIDIA GeForce 8800 GTX. The second non-standard component is the height-ridge traversal procedure (see Sec. 2) that is computationally highly efficient. Even for large datasets containing many tubular objects the computation times are below one second. Thus, using a GPU based implementation of the GVF, the whole processing pipeline can be computed on a standard workstation within times comparable to some pure skeletonization approaches [2,4], exclusive of the additional computation times these methods require for the segmentation step.

4 Conclusion

In this work we presented an approach for extraction of CSs directly from gray value images. The approach combines the advantages of a bottom up tube detection filter with the GVF's ability for extraction of medial curves also in cases where the objects are not tubular. This combination enables robustness against local disturbances such as stenoses/aneurisms along the tubes and an extraction of medial curves also in these areas. We demonstrated the applicability of our approach on various clinical datasets and showed that the accuracy of the resulting centerline is comparable to that achieved with state of the art skeletonization approaches that are all based on the same known segmentations. Thus, the final CSs extracted with our approach are directly applicable for VE applications and

[1] `www.itk.org`
[2] `www.nvidia.com/object/cuda_home.html`

other application areas that require CS extraction and this supersedes the need to deal with segmentations and skeletonizations.

Acknowledgements. The authors thank Univ.Doz.Dr. Erich Sorantin from the Dep. of Radiology, Medical University Graz, Austria, and Prof.Dr.-Ing. Georgios Sakas for providing the clinical datasets.

References

1. Palagyi, K., Sorantin, E., Balogh, E., Kuba, A., Halmai, C., Erdohelyi, B., Hausegger, K.: A sequential 3D thinning algorithm and its medical applications. In: Insana, M.F., Leahy, R.M. (eds.) IPMI 2001. LNCS, vol. 2082, pp. 409–415. Springer, Heidelberg (2001)
2. Hassouna, M.S., Farag, A.A.: On the extraction of curve skeletons using gradient vector flow. In: Proc. of ICCV, pp. 1–8 (2007)
3. Hassouna, M.S., Farag, A.A., Falk, R.: Differential fly-throughs (DFT): A general framework for computing flight paths. In: Duncan, J.S., Gerig, G. (eds.) MICCAI 2005. LNCS, vol. 3750, pp. 654–661. Springer, Heidelberg (2005)
4. Bouix, S., Siddiqi, K., Tannenbaum, A.: Flux driven automatic centerline extraction. MIA 9(3), 209–221 (2005)
5. Deschamps, T., Cohen, L.D.: Fast extraction of minimal paths in 3d images and applications to virtual endoscopy. MIA 5(4), 281–299 (2001)
6. Wink, O., Niessen, W., Viergever, M.: Multiscale vessel tracking. IEEE TMI 21(2)23(1), 130–133 (2004)
7. Aylward, S., Bullit, E.: Initialization, noise, singularities, and scale in height ridge traversal for tubular object centerline extraction. IEEE TMI 21(2), 61–75 (2002)
8. Krissian, K., Malandain, G., Ayache, N., Vaillant, R., Trousset, Y.: Model-based detection of tubular structures in 3D images. CVIU 2(80), 130–171 (2000)
9. Frangi, A.F., Niessen, W.J., Vincken, K.L., Viergever, M.A.: Multiscale vessel enhancement filtering. In: Wells, W.M., Colchester, A.C.F., Delp, S.L. (eds.) MICCAI 1998. LNCS, vol. 1496, pp. 130–137. Springer, Heidelberg (1998)
10. Bullitt, E., Aylward, S., Smith, K., Jukherji, S., Jiroutek, M., Muller, K.: Symbolic description of intracerebral vessels segmented from magnetic resonance angiograms and evaluation by comparision with x-ray angiograms. MIA 5(2), 157–169 (2001)
11. Szymczak, A., Stillman, A., Tannenbaum, A., Mischaikow, K.: Coronary vessel trees from 3d imagery: A topological approach. MIA 10(4), 548–559 (2006)
12. Bauer, C., Bischof, H.: A novel approach for detection of tubular objects and its application to medical image analysis. In: Proc. of DAGM 2008 (in print) (2008)
13. Xu, C., Prince, J.L.: Snakes, shapes, and gradient vector flow. IEEE TMI 7(3), 359–369 (1998)